

Additional on-line material for paper “A comprehensive set of simulations of high-velocity collisions between main sequence stars”.

Marc Freitag^{1,2*}, and Willy Benz^{3†}

¹*Observatoire de Genève, Chemin des Maillettes 51, CH-1290 Sauverny, Switzerland*

²*Astronomisches Rechen-Institut, Mönchhofstraße 12-14, D-69120 Heidelberg, Germany*

³*Universität Bern, Sidlerstrasse 5, CH-3012 Bern, Switzerland*

Accepted. Received; in original form

ABSTRACT

We present various plots to complement our paper “A comprehensive set of simulations of high-velocity collisions between main sequence stars”. The density profiles for the stellar models are plotted and compared to polytropic models. We show how the SPH particle configurations realise them. For illustrative purposes, we present in detail a few particular collision simulations. Finally, typical mass and energy loss curves are shown.

Key words: hydrodynamics – methods: numerical – stars: interior – galaxies: nuclei, star clusters – Galaxy: centre

1 SMOOTHED PARTICLE HYDRODYNAMICS STELLAR MODELS.

1.1 Stellar structure used in the simulations

In Fig. 1, we show the density profiles for some realistic models for MS stars and compare them with polytropic stars. It is readily seen that for $M > 0.4 M_{\odot}$, stellar structures are highly non-homologous and that polytropes do not match, even if allowance is made for a M -variable n index. If such a fit is required anyway, a value of $n \simeq 3.5$ seems more appropriate for $M \geq 1 M_{\odot}$ than the commonly used $n = 3$.

An SPH particle configuration for a star is illustrated on Fig. 2. One sees that the outermost layers of the star are very poorly modelled, with a clear failure at precisely reproducing the real stellar radius. Fig. 3 is a comparison between the density and internal energy profiles of two stellar models and their SPH approximation for increasing number of particles.

1.2 Choice of the particle number

In Fig. 4, we show how the overall results of SPH collision simulations (mass and energy loss, deflection angle) depend on the resolution, i.e. the number of particles used to represent the stars. We considered resolution ranging from 1000+2000 to 2000+32 000 particles.

* E-mail: freitag@ari.uni-heidelberg.de. Present address: Department of Physics and Astronomy, Northwestern University, 2145 Sheridan Road, Evanston, IL 60208-0834, USA

† E-mail: willy.benz@phim.unibe.ch

2 RESULTS OF SPH SIMULATIONS

2.1 A few specific collision simulations

Precise descriptions of the physical mechanisms at play during stellar collisions have already been published (Benz & Hills 1987, 1992; Lai et al. 1993; Lombardi et al. 1996). In this subsection, we just highlight a few particular collisions from our survey for illustration purposes. We do not particularly concentrate on “classical” typical cases because they have been well covered in these previous works. Instead, we concentrate on simulations with parameters lying on the border-lines of the various regimes. Many of them have been re-computed in order to test surprising results. Indeed, for lack of sufficient disk space for data storage, only the final “state” of each SPH simulation was conserved for most runs. So, when any doubtful result appeared, we had to re-compute the complete simulation and write the data to disk frequently in order to understand the evolution of the system.

In Fig. 5, we show an off-axis low velocity encounter between identical stars. As the impact parameter is small, the stars merge together after the first periastron passage. The colour mapping used in these diagrams allow to trace each particle back to its initial radial position in the colliding stars. Despite the rather low resolution (about 8000 particles in total) a tighter and tighter spiral pattern is clearly visible. As explained by Lombardi and collaborators, in low velocity collisions, specific entropy s is nearly conserved as shock heating is weak, and, as stability of the resulting star imposes $ds/dr > 0$, low entropy material that was initially

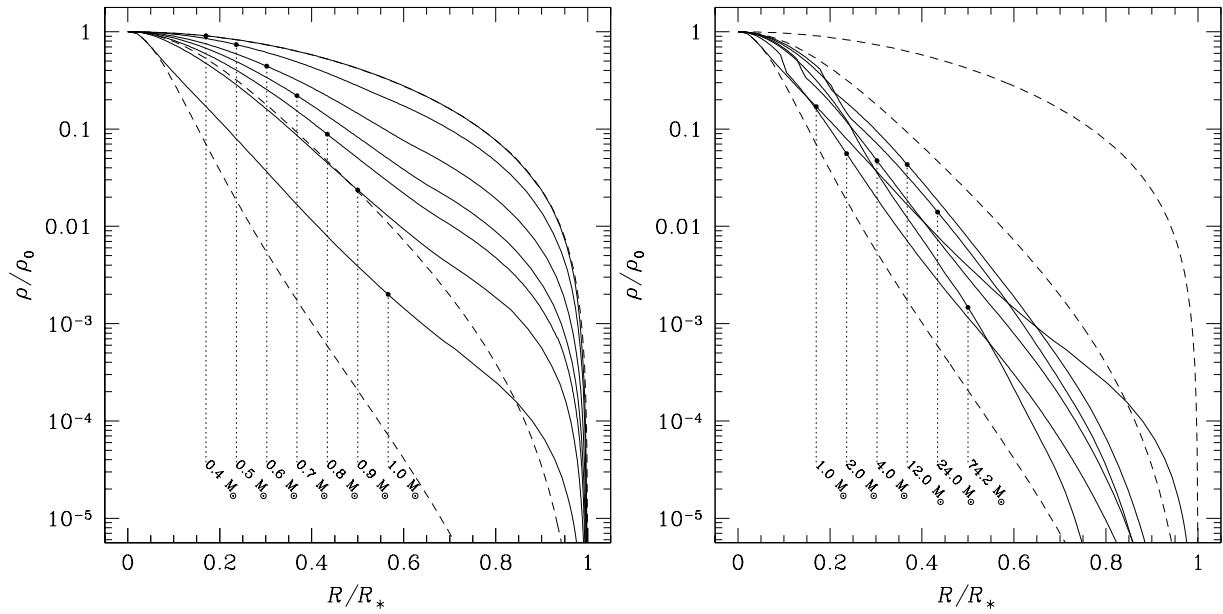


Figure 1. Density profiles for realistic star models (Schaller et al. 1992; Charbonnel et al. 1999) for low (top) and high (bottom) mass stars. The dashed lines are polytropic models for $n = 1.5, 3$ and 4 , in order of increasing concentration. Below $0.4 M_{\odot}$, the density structure is well represented by a polytrope with $n = 1.5$ but no good polytropic fit is possible for higher masses.

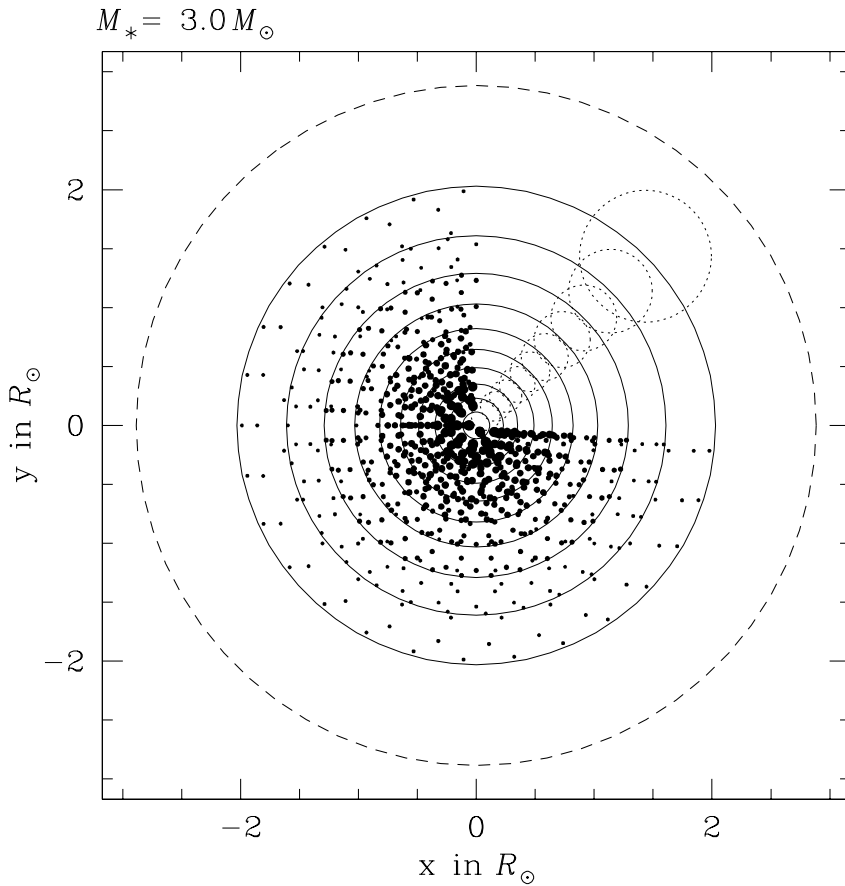


Figure 2. SPH realisation of a $3 M_{\odot}$ stellar model with ~ 2000 particles. Round dots show the positions of SPH particles with a symbol surface proportional to the particle's mass. The big dashed circle shows the size of the star according to the structure model. Plain line circles depict the concentric spheres on the surface of which the particles' centres are placed. Particles on the $x, y > 0$ corner of the diagram have been removed to show the actual half-size of particles on each sphere (dotted circles of radius h).

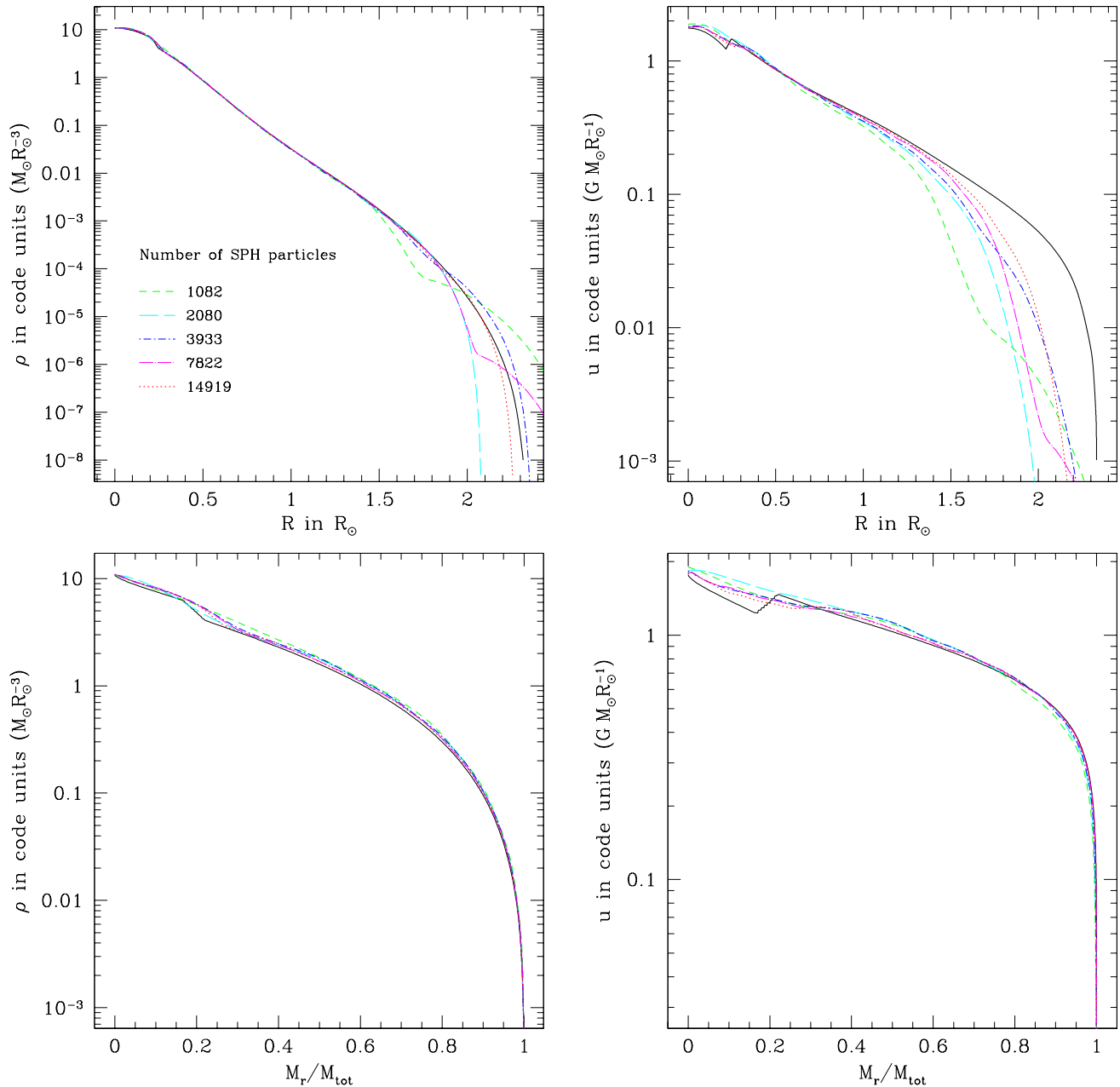


Figure 3. Comparison between the theoretical internal structure of a $2 M_{\odot}$ stellar model (solid lines) and SPH realisations of it with increasing number of particles (dashed and dotted lines). We show the mass density (left column) and the internal energy (right column). In the top row, we use the radius as the abscissa, while we use the enclosed mass for the diagrams of the bottom row. The top plots show that the outermost part of the star are poorly represented. However, it is clear from the bottom plots that only a tiny mass fraction suffers from this mismatch. The SPH profiles are the kernel-interpolated values along the line $z = 0$.

at the centre of the stars, settles in the centre of the merged object. In fact, for such gentle encounters, one can even predict the final material stratification by sorting mass elements from the two stars in order of increasing entropy (Lombardi et al. 1996, 2002, 2003). A consequence of this mechanism is that, in mergers between stars with unequal masses, the core of the smaller one, having the lowest entropy, sinks to the centre of the merger. This is also what happens in the two collisions depicted in Figures 6, 7 and 8. The second collision is an example of a high velocity merger which produce an object with a total mass slightly *lower*

than those of the initial larger star. Such a case lies in the tip of merger region in a diagram like those in Fig. 9 of the main paper.

In Figures 9 and 10, we display snapshots from one of the few head-on collisions in which the small star pass through the large one and remains essentially intact. A further peculiarity of this collision is its relatively large mass ratio: $q = 0.24$. No collision with a larger q resulted in a similar outcome. Figures 11 and 12 depict a more typical “fly-by” in the sense that it has non-vanishing impact parameter. However, this high velocity encounter lies very close

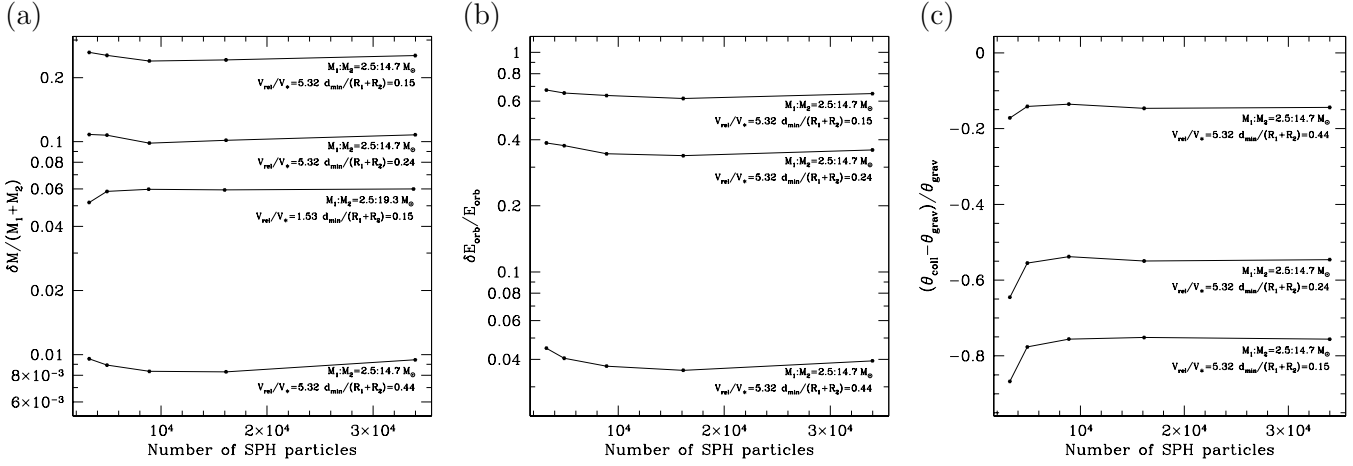


Figure 4. Study of the dependency of collision results on the particle number for 4 sets of collision simulations. (a) Fractional mass loss. (b) Fractional loss in orbital energy. The simulation set with $M_2 = 19.3 M_\odot$ is not reported here because it results in a merger ($\delta E_{orb}/E_{orb} = 1$). (c) Deviation of the collisional deflection angle θ_{coll} from the value for pure Keplerian point-mass trajectory θ_{grav} .

to the strip of complete disruption of the small star. For this particular simulation, the small star loses more than 89% of its mass! The remaining cloud has a very low central density, around $10^{-4} \text{ g cm}^{-3}$. It is made of only 187 particles so simulations with higher resolution are clearly needed to confirm that the production of such tiny survivors is not a numerical artifact. It is however unlikely that such small, rarely formed objects, may have important astrophysical relevance, either as detectable “exotic” stars or dynamically.

We finally present a collision from the high velocity, 1-star branch, i.e. a case of collisionally induced evaporation of the small star. We particularly checked that this kind of outcome was real and not some artifact cause by our analysis software. Indeed, during these verifications, we noted that many cases of nearly complete destruction of the small star like the one described in Figures 9 and 10 were misinterpreted because our code missed the second, much lower, density peak. Consequently, we had to re-analyse all high ν collisions that were reported to result in the disruption of the small star. We conclude that although the precise location of its right (large d_{min}) edge may depend on numerical issues (resolution, analysis procedure), the 1-star branch is real. Inspecting the last frames of Figures 13 and 14 and Fig. 15 makes this fact obvious. Furthermore, such collision results have been reported by Lai et al. (1993).

2.2 Examples of mass and energy loss results

Fig. 16 shows the energy and mass loss curves for the simulations of collisions between stars with $(M_1, M_2) = (0.5, 12) M_\odot$, and $(12, 12) M_\odot$. Similar curves for other (M_1, M_2) couples are available upon request to MF. The can also easily be drawn using the complete tables of collision results available on-line.

REFERENCES

- Benz W., Hills J. G., 1987, ApJ, 323, 614
 —, 1992, ApJ, 389, 546

- Charbonnel C., Däppen W., Schaerer D., Bernasconi P. A., Maeder A., Meynet G., Mowlavi N., 1999, A&AS, 135, 405
 Lai D., Rasio F. A., Shapiro S. L., 1993, ApJ, 412, 593
 Lombardi J. C. J., Rasio F. A., Shapiro S. L., 1996, ApJ, 468, 797
 Lombardi J. C., Thrall A. P., Deneva J. S., Fleming S. W., Grabowski P. E., 2003, MNRAS, 345, 762
 Lombardi J. C., Warren J. S., Rasio F. A., Sills A., Warren A. R., 2002, ApJ, 568, 939
 Schaller G., Schaerer D., Meynet G., Maeder A., 1992, A&AS, 96, 269

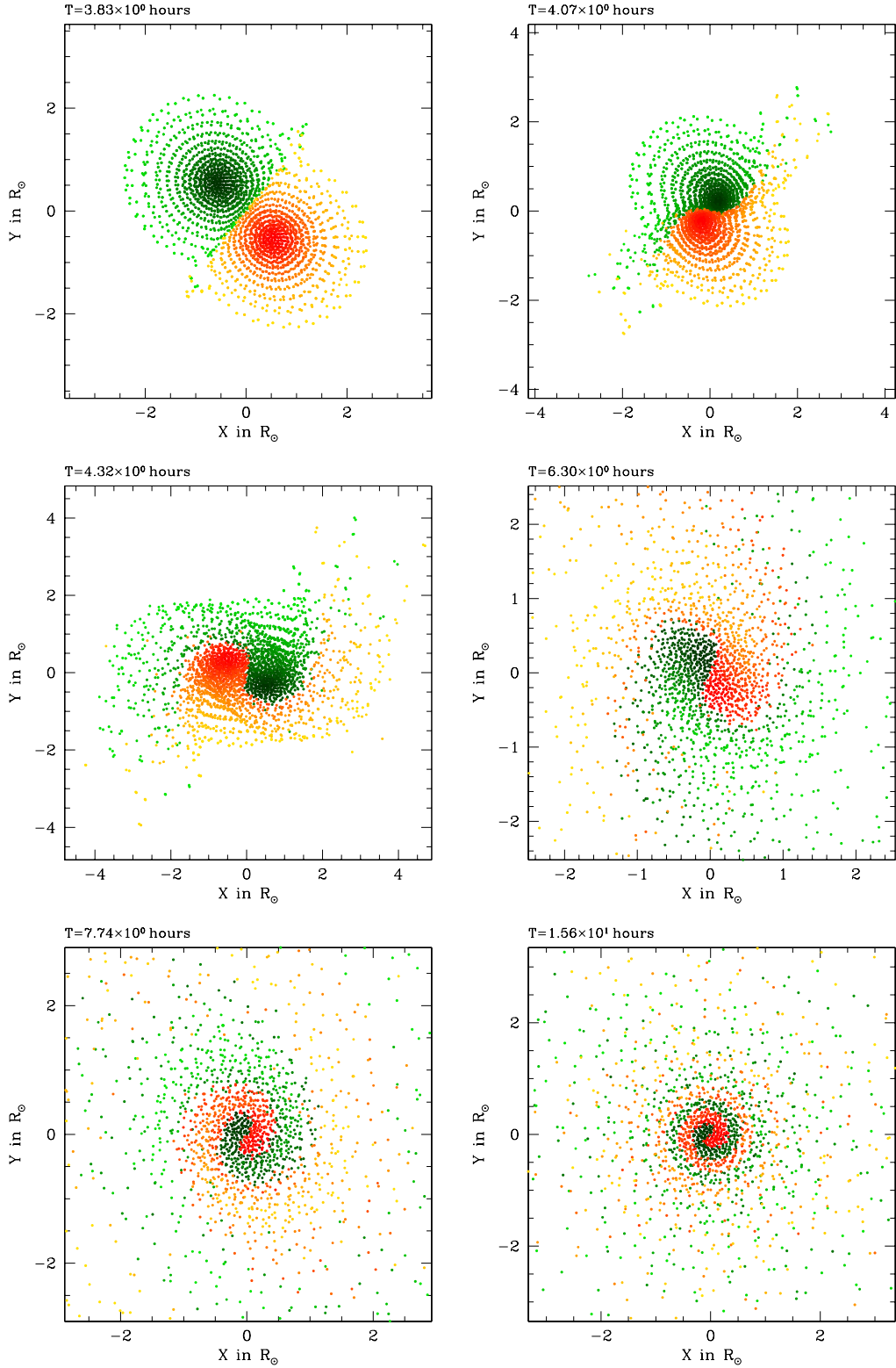


Figure 5. Collision between two $2.0 M_{\odot}$ stars at $V_{\text{rel}}^{\infty}/V_{*} = 0.77$ (465 km s^{-1}) and $d_{\text{min}}/(R_1 + R_2) = 0.1$. Each plot show the position, projected onto the orbital plane, of SPH particles that lie close to this plane. Beware that the length scale may change from frame to frame. This collision creates a merged star with mass $3.81 M_{\odot}$. The particles are colour-coded according to their rank in the initial stellar models.

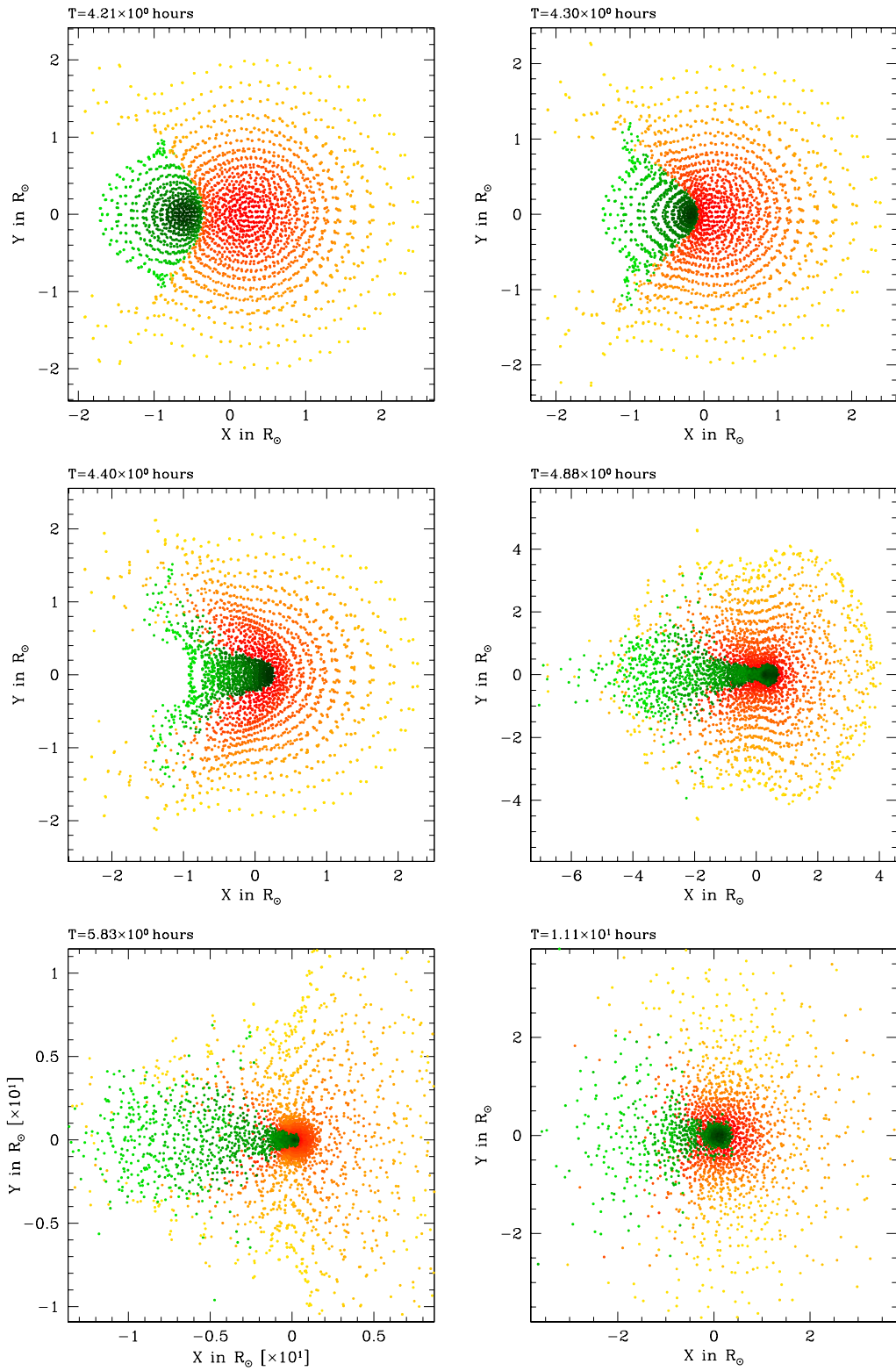


Figure 6. Collision between stars of masses 1.0 and $3.0 M_{\odot}$ at $V_{\text{rel}}^{\infty}/V_{*} = 0.07$ (44 km s^{-1}) and $d_{\text{min}}/(R_1 + R_2) = 0.0$. This collision creates a merged star with mass $3.80 M_{\odot}$. The particles are colour-coded according to their rank in the initial stellar models.

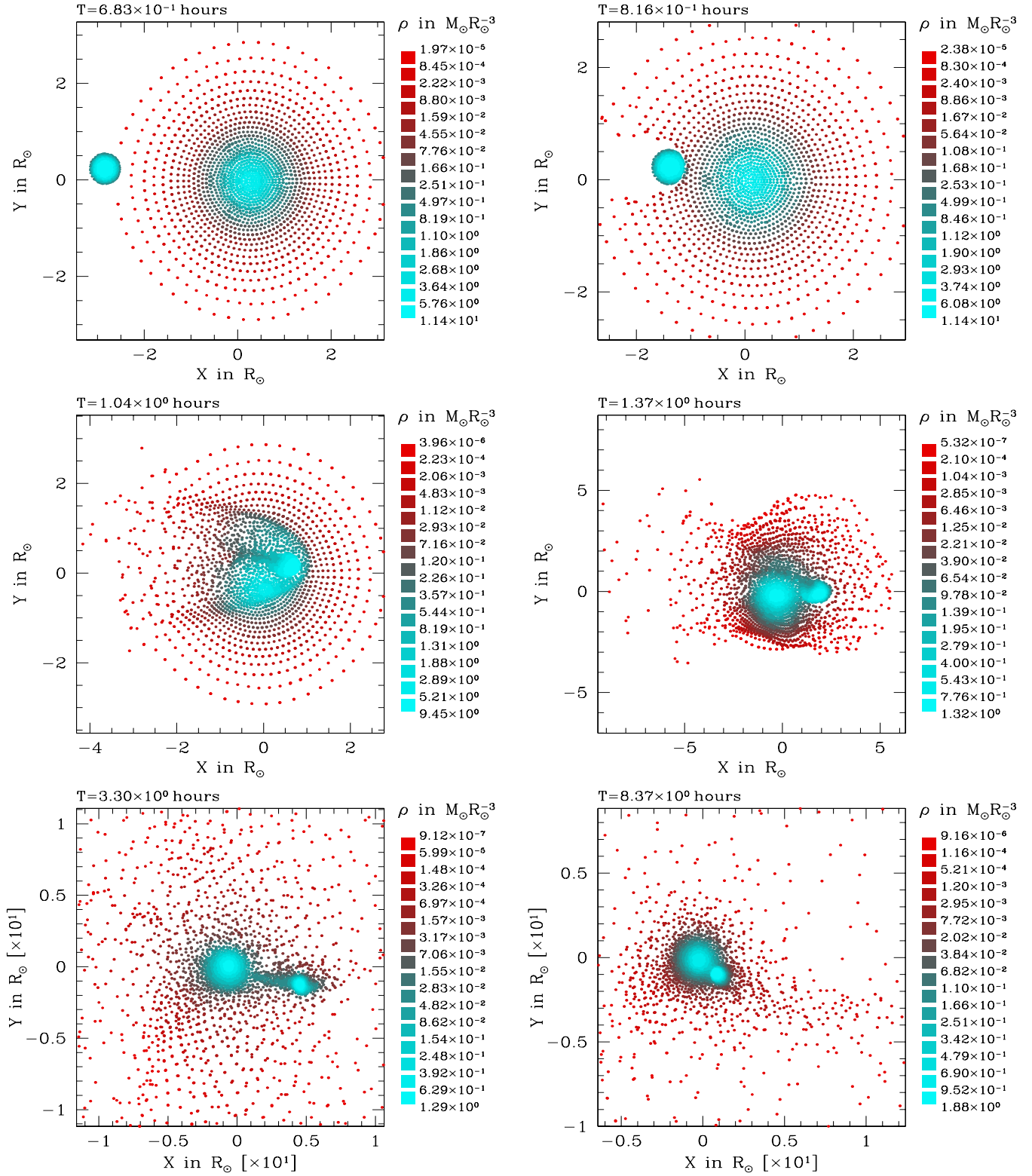


Figure 7. Collision between stars of masses $0.4 M_{\odot}$ and $4.0 M_{\odot}$ at $V_{\text{rel}}^{\infty}/V_{*} = 3.24$ (2180 km s^{-1}) and $d_{\text{min}}/(R_1 + R_2) = 0.04$. The colours code the gas density. This collision results in a merged star with mass $3.75 M_{\odot}$.

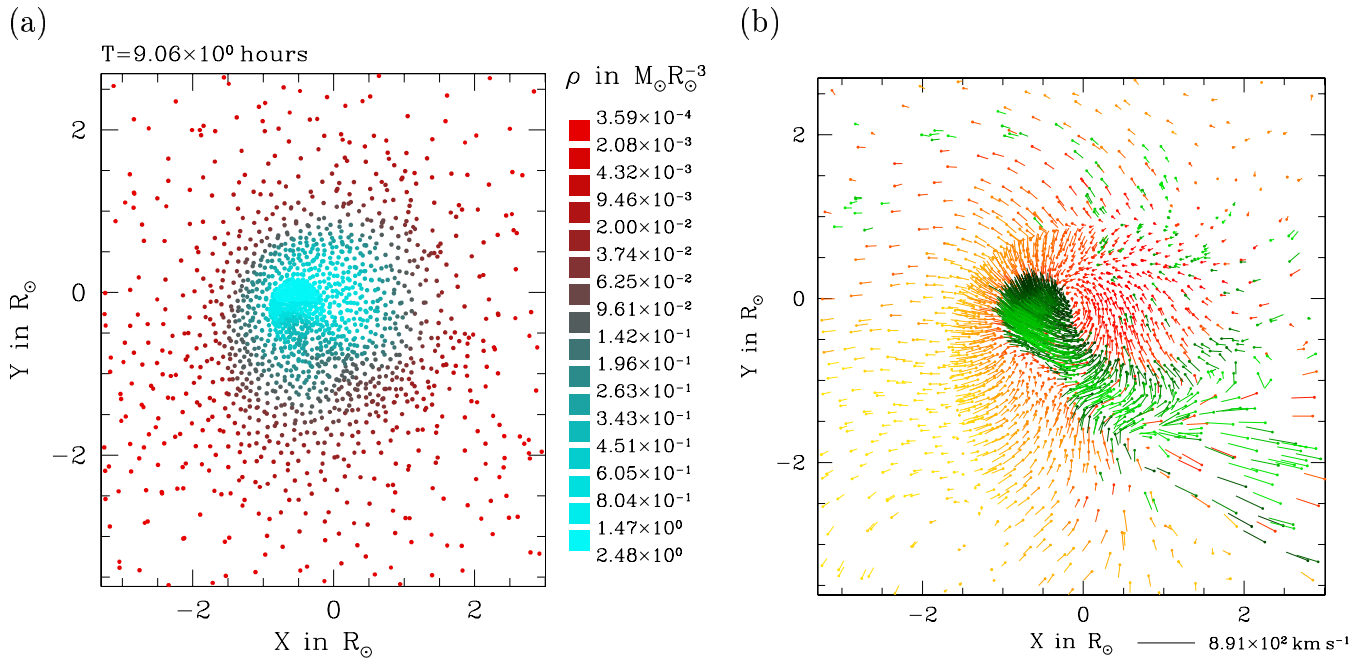


Figure 8. Snapshot of the collision simulation of Fig. 7 at later stage. One sees the small star spiralling into the centre of the larger star. Panel (a): density plot. Panel (b): Velocity plot with colours indicating the radial position of each particle in the initial stellar models. Particles from the large star are coded in red to yellow, from centre to surface. Particles from the small star are coded in dark to light green. The small dots are the position of the particles. The velocity scale is given by the horizontal line segment at the bottom right of the diagram.

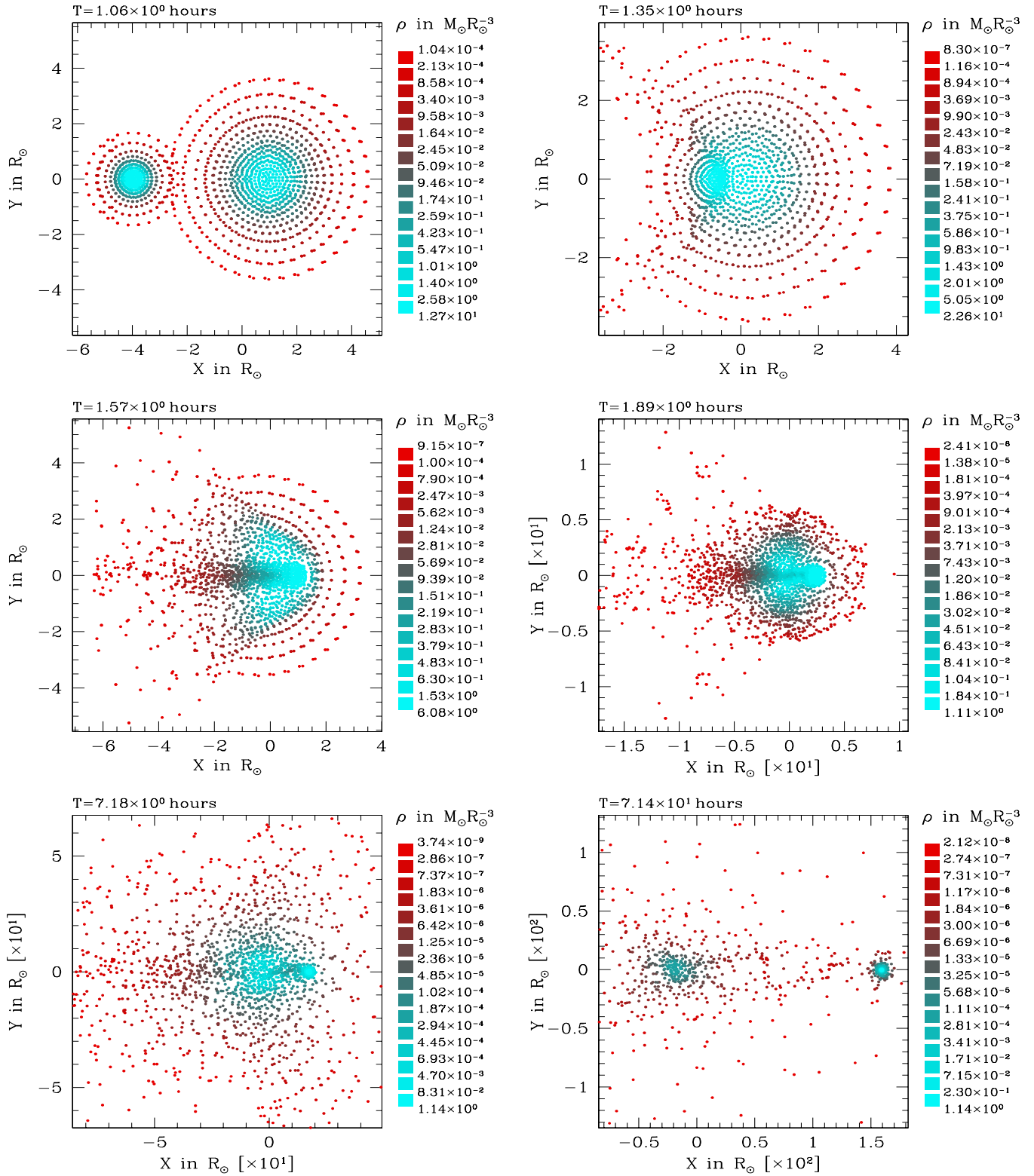


Figure 9. Collision between stars of masses $1.7 M_{\odot}$ and $7.0 M_{\odot}$ at $V_{\text{rel}}^{\infty}/V_{*} = 3.68$ (2620 km s^{-1}) and $d_{\text{min}}/(R_1 + R_2) = 0.0$. Not only is the small star still bound as it emerges from the collision, but it has also accreted some gas from the larger star so that its final mass is $1.74 M_{\odot}$! Much damage has been caused to the larger star, though, which has lost all but $1.94 M_{\odot}$.

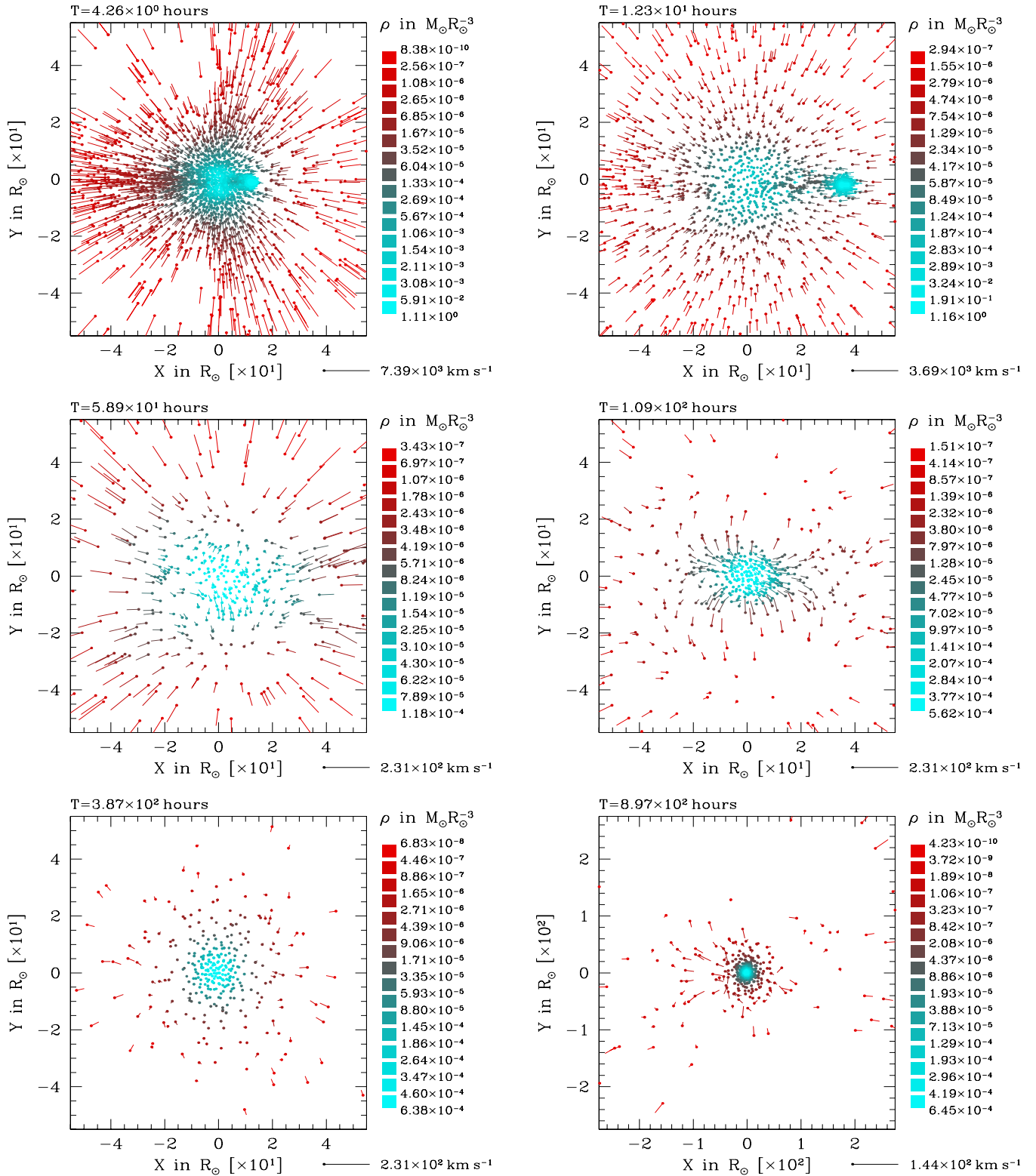


Figure 10. Same collision as in Fig. 9. In this series of plots, Positions and densities are relative to the particle that lies at the centre of the larger star at the end of the simulations. A constant length scale is applied to all diagrams but the last one which shows a larger view. The velocity scale is adapted from frame to frame.

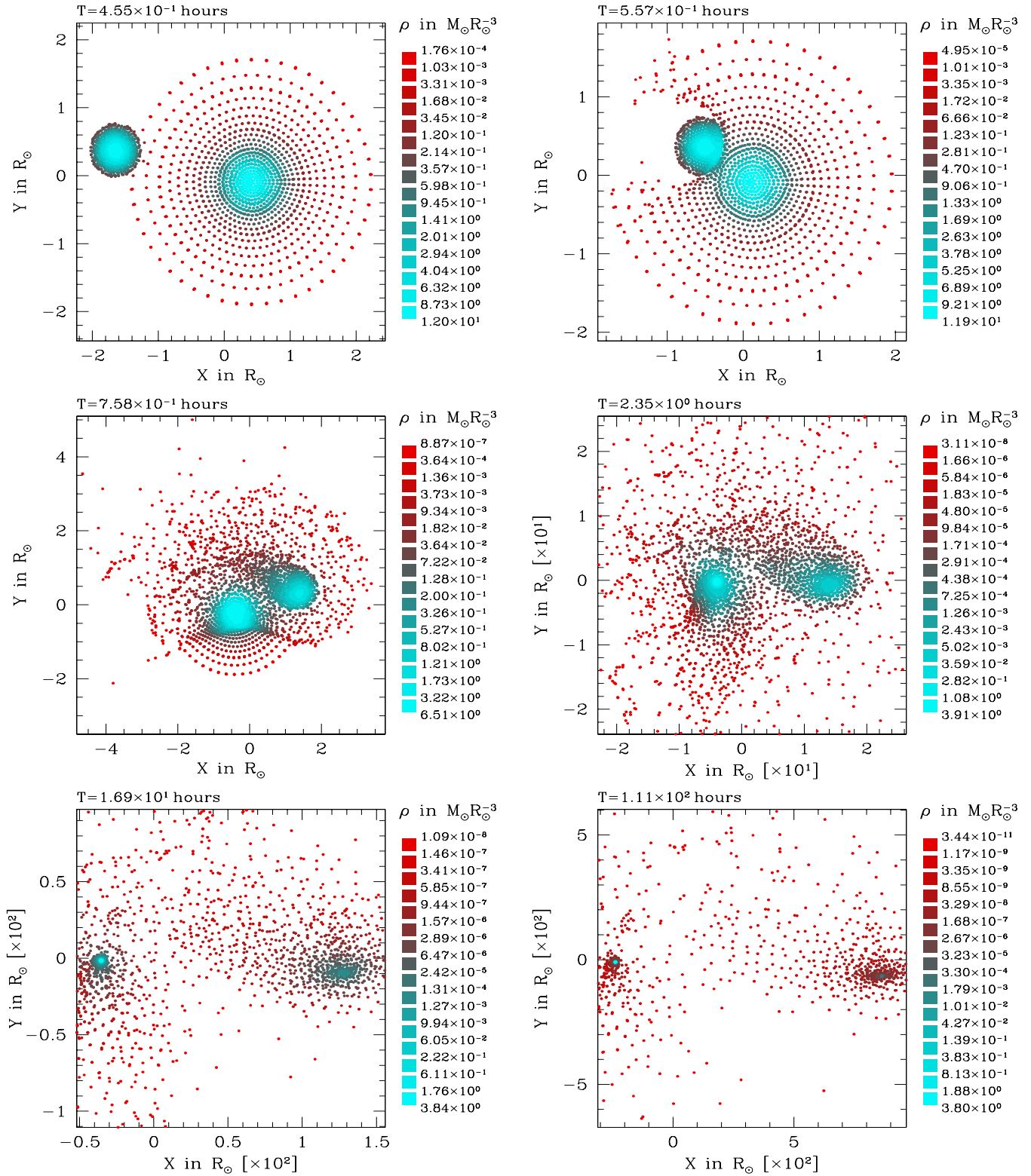


Figure 11. Collision between stars of masses $0.5 M_{\odot}$ and $2.0 M_{\odot}$ at $V_{\text{rel}}^{\infty}/V_{*} = 4.48$ (2620 km s^{-1}) and $d_{\text{min}}/(R_1 + R_2) = 0.15$.

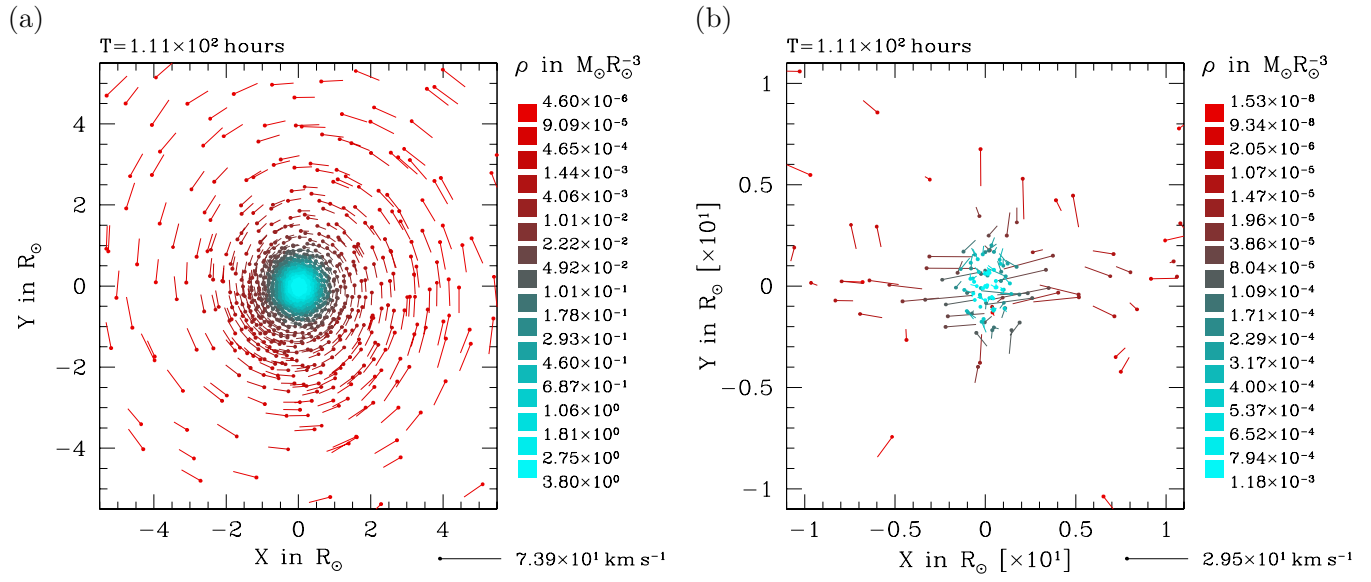


Figure 12. Enlargements of the last frame of Fig. 11. Position and velocities are relative to the particle with the highest density in each panel. Panel (a): remaining of the large star ($1.53 M_\odot$). Panel (b): remaining of the small star ($0.05 M_\odot$).

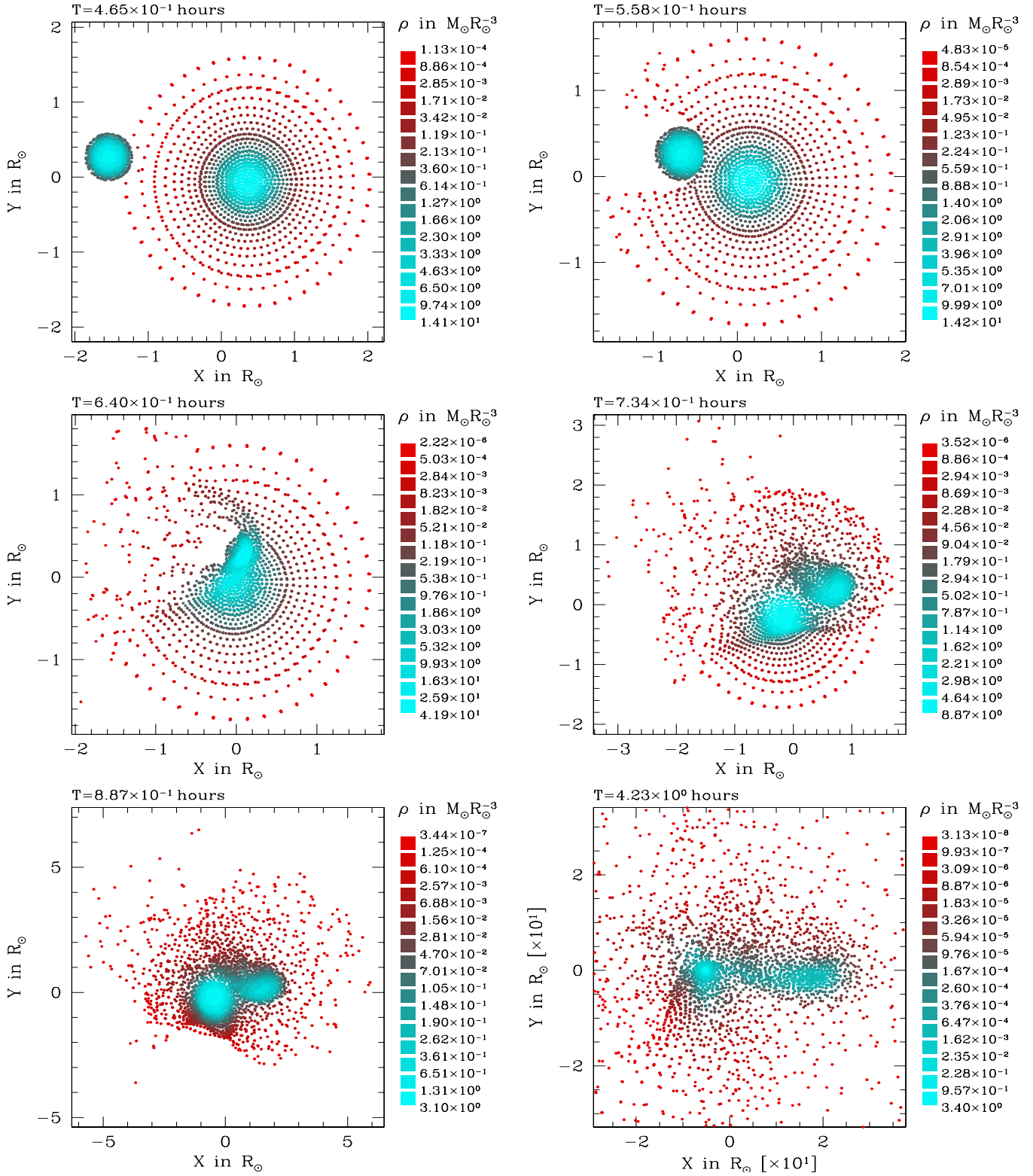


Figure 13. Collision between stars of masses $0.4 M_{\odot}$ and $1.7 M_{\odot}$ at $V_{\text{rel}}^{\infty}/V_{*} = 3.80$ (2180 km s^{-1}) and $d_{\text{min}}/(R_1 + R_2) = 0.11$.

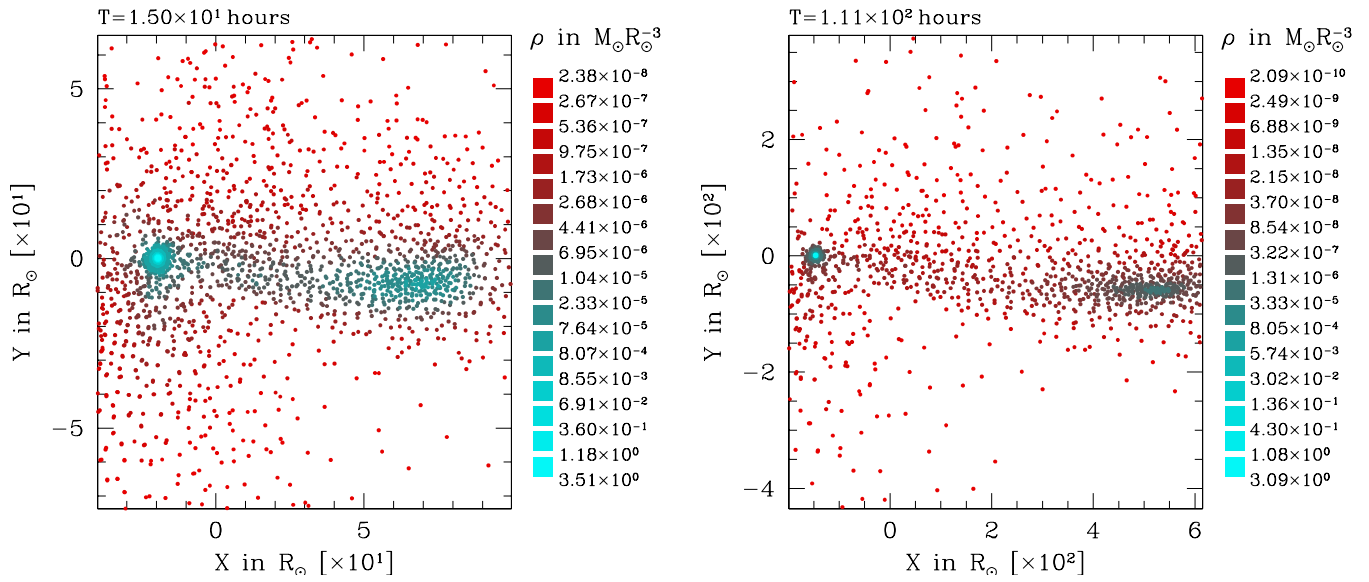


Figure 14. Continuation of the sequence of Fig. 13.

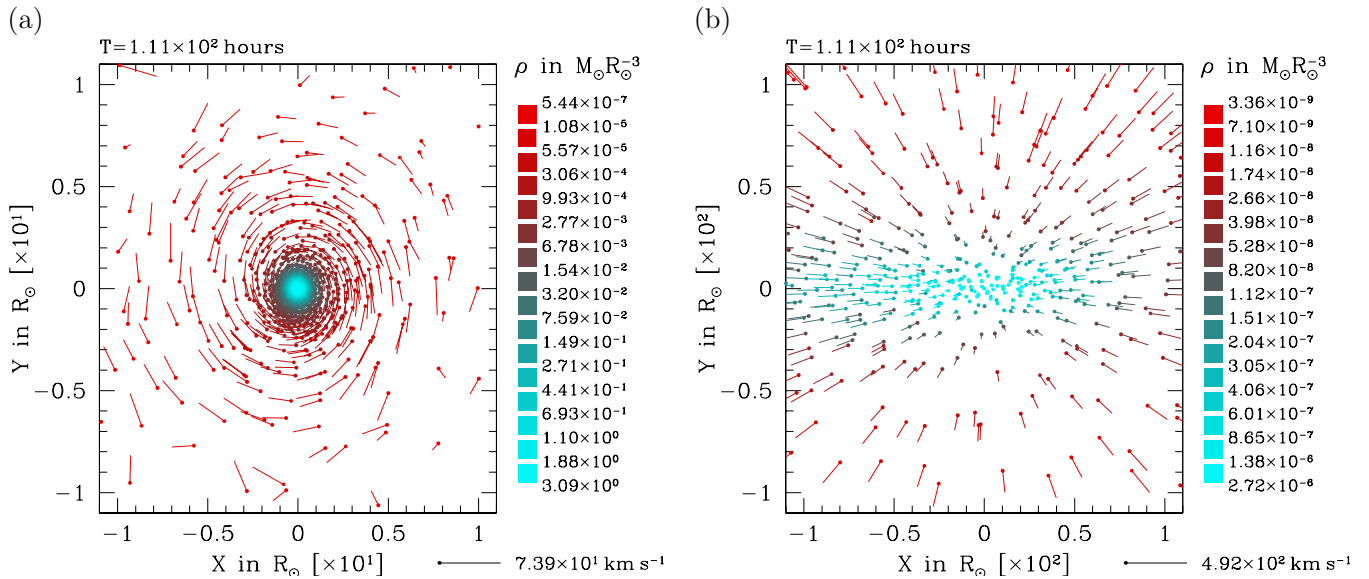


Figure 15. Enlargements of the last frame of Fig. 14. Position and velocities are relative to the particle with the highest density in each panel. Panel (a): surviving core of the large star, a $1.26 M_{\odot}$ rotating star. Panel (b): remaining of the core of the small star, an unbound expanding gas cloud. The velocity of this cloud in the centre-of-mass reference frame of the collision is nearly 1000 km s^{-1} while the velocity of the small star was initially 1770 km s^{-1} .

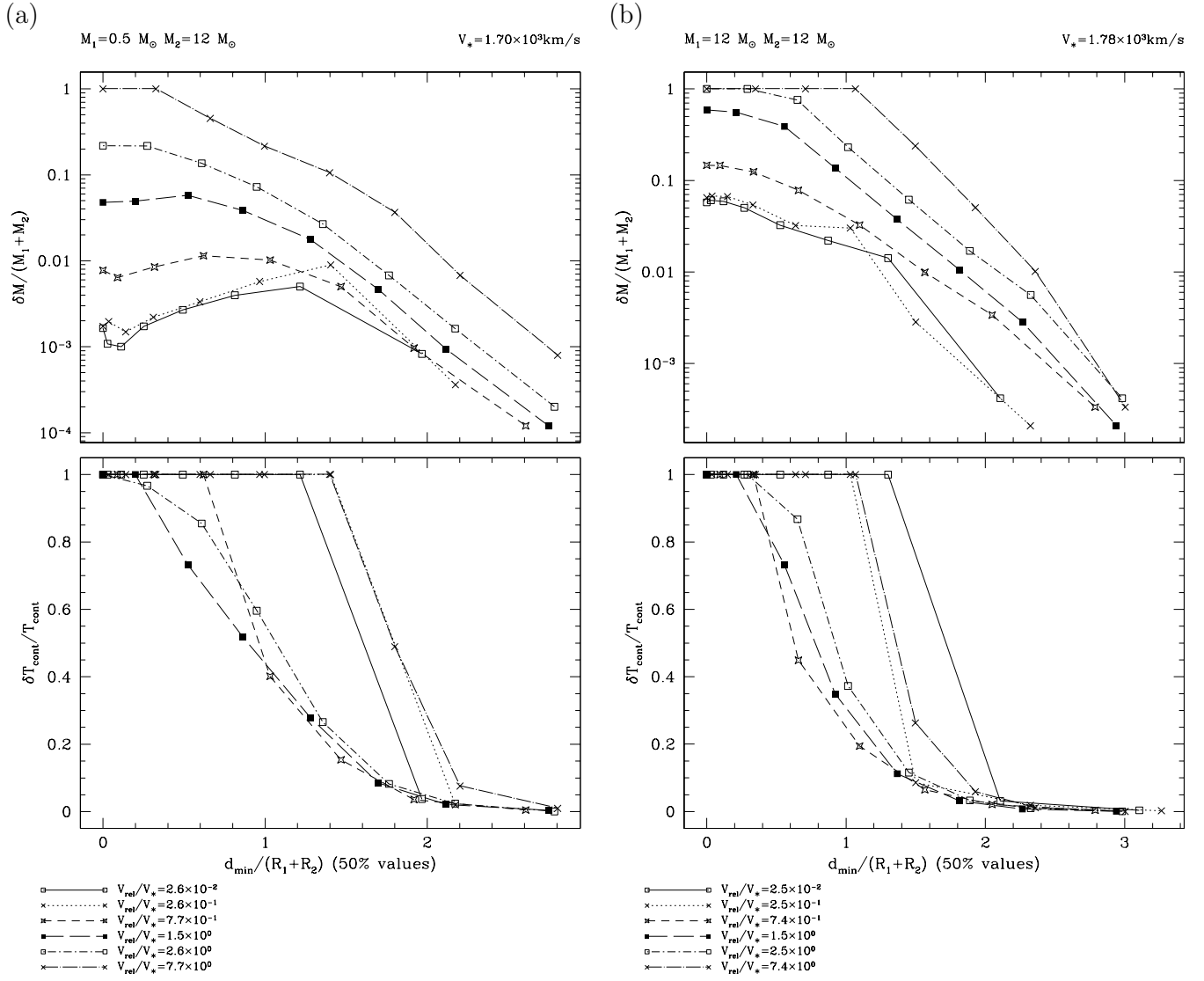


Figure 16. Relative mass and kinetic energy losses for all collision simulations between stars of masses 0.5 and $12 M_\odot$ (column (a)) and 12 and $12 M_\odot$ (column (b)). Half-mass radii are used to normalise parameters. T_{cont} is the orbital kinetic energy at “half-mass contact” (separation equal to $R_1^{(h)} + R_2^{(h)}$), assuming purely Keplerian acceleration. For very small V_{rel}^∞ , all encounters result either in mergers or in bound binaries that should eventually merge together, with $\delta T_{\text{cont}}/T_{\text{cont}} = 1$ and a higher $\delta M/(M_1 + M_2)$ as consequences. At high velocities, the domain of 100% complete energy loss extends to d_{min} values where mass loss is only partial. This is due to the complete disruption of the smaller star after it emerges from the large one. The shoulders on the low velocity mass loss curves are due to the formation and subsequent merging of a binary.